Effects of nitrate radical levels and pre-existing particles on secondary brown carbon formation from nighttime oxidation of furan

Kunpeng Chen,[1] Raphael Mayorga,[2] Nilofar Raeofy,[1] Michael Lum,[1] Megan Woods,[2] Roya Bahreini,[1] Haofei Zhang,[2] Ying-Hsuan Lin[1,*]

[1]Department of Environmental Sciences, University of California, Riverside, California 92521, United States

[2]Department of Chemistry, University of California, Riverside, California 92521, United States

ABSTRACT

Furans are predominant heterocyclic volatile organic compounds (VOCs) in the atmosphere from both primary and secondary sources, such as direct emissions from wildfires and atmospheric oxidation of dienes. Formation of secondary organic aerosols (SOA) from the oxidation of furans has been reported. Previous research has shown that furan SOA generated from nighttime oxidation contributes to brown carbon (BrC) formation; however, how nighttime oxidant levels (represented by nitrate radical (NO_3) levels) and pre-existing particles influence the SOA chemical composition and BrC optical properties is not well constrained. In this study, we conducted chamber experiments to systematically investigate the role of these two environmental factors in furan-derived secondary BrC formation during the nighttime. Our results suggest that the bulk compositions of SOA measured as ion fragment families by an aerosol mass spectrometer (mAMS) are unaffected by changes in NO_3 levels, but can be influenced by the presence of pre-existing ammonium sulfate particles. Based on the mass absorption coefficient (MAC) profiles of SOA produced under different experimental conditions, the BrC light absorption was enhanced by higher NO_3 levels and reduced by the presence of pre-existing ammonium sulfate seed particles, suggesting that NO_3-initiated oxidation of furan can promote the formation of light-absorbing products while pre-existing particles may facilitate the partitioning of non-absorbing organics in the aerosol phase. Furthermore, molecular-level compositional analysis reveals a similar pattern of chromophores under various studied environmental conditions, in which highly oxygenated monomers (e.g., $C_4H_4O_6$ and $C_4H_3NO_7$), dimers, and oligomers can all contribute to BrC chromophores. Taken together, the NO_3 levels and pre-existing particles can influence secondary BrC formation by altering SOA compositions, which is critical for assessing BrC optical properties in a complex environment.

KEYWORDS nighttime oxidation, NO_3-initiated reactions, NO_3 levels, pre-existing particles, highly oxygenated chromophores

TOC Graphic

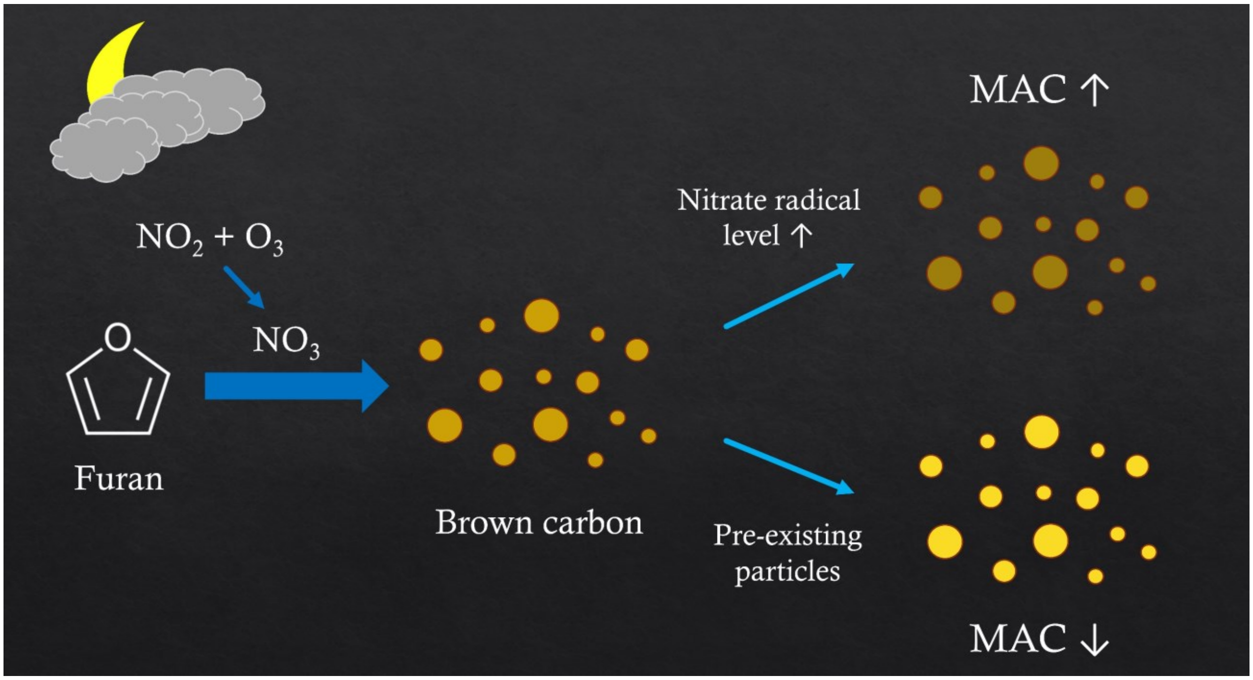

$NO_2 + O_3$
NO_3
Furan
Brown carbon
Nitrate radical level ↑
Pre-existing particles
MAC ↑
MAC ↓

INTRODUCTION

Heterocyclic volatile organic compounds (VOCs) are a class of ubiquitous but understudied precursors of secondary organic aerosols (SOA) that have a substantial impact on air quality and the solar radiative budget of the Earth. Heterocyclic VOCs emitted from biomass burning[1-3] are expected to become increasingly important due to the combustion of fossil fuels[4, 5] and the increased wildfire episodes with global warming.[6-8] Because of the heteroatoms, heterocyclic VOCs with aromatic rings exhibit distinctive reactivity when compared to the homocyclic compounds (e.g., toluene, naphthalene), and thus their fates in atmospheric oxidation have gained increasing attention. In particular, furans are common heterocyclic VOCs that are released when cellulose and hemicellulose are pyrolyzed during biomass burning,[9-11] especially when burning wiregrass,[12] and are often observed in field measurements.[3, 13, 14] Furans are also secondary products of atmospheric hydroxyl radical (OH)-initiated oxidation of dienes (e.g., butadiene and isoprene).[15-17] Recent research suggested that furans may contribute to around 20-30% of SOA generated in biomass burning,[18, 19] highlighting the crucial role of furans as SOA precursors.

The gas-phase oxidation pathways of furans are widely studied and have been incorporated into mechanistic models,[20, 21] whereas the aerosol-phase compositions are less well-defined. Alvarez et al.[22] reported that OH-initiated oxidation of furans can produce a large set of unsaturated 1,4-dicarbonyls in the aerosol phase, while Joo et al.[23] suggested that nitrate radical (NO_3)-initiated oxidation of 3-methylfuran can not only generate a variety of carbonyls but also dimers and oligomers. Strollo and Ziemann[24] indicated that oligomerization is the key to SOA formation during 3-methylfuran daytime oxidation, while Jiang et al.[25] highlighted the potentially important role of multifunctional dihydroxyl organonitrate products in SOA formation in the furan-

NO_x-NaCl system. However, our understanding of the chemical composition of reaction products in furan oxidations is still limited, making it difficult to evaluate the physicochemical properties of furan SOA.

The optical properties of aerosols, in particular, are critical for influencing atmospheric radiative balance,[26] but the optical properties of furans SOA have not been thoroughly investigated. Grace et al.[27] suggested that furan derivatives in aqueous aerosols could potentially contribute to the formation of brown carbon (BrC), which is defined as the light-absorbing organic matter in aerosols. Jiang et al.[28] reported that nighttime oxidation of furan can produce secondary BrC. Even though furans have been shown to be a precursor of SOA and BrC, it is unclear how environmental conditions regulate furan SOA and BrC formation. Tsigaridis and Kanakidou[29] hypothesized that oxidant levels (i.e., concentration of oxidants) and pre-existing particles are two crucial environmental factors that will influence the future SOA burden in the atmosphere. Oxidant levels are anticipated to affect the oxidation products and, consequently, the optical properties of SOA,[30] whereas pre-existing particles may alter the amount of SOA constituents by facilitating gas-particle partitioning and heterocyclic reactions. However, the relationship between these processes and BrC formation has not been thoroughly investigated. Since furans can contribute to 5-37% of the emitted VOCs in biomass burning smoke,[3, 10] it is essential to constrain the role of oxidant levels and pre-existing particles in the formation of BrC from the oxidation of furans under various environmental conditions.

In this study, chamber experiments were carried out to determine the effects of oxidant levels and the presence of pre-existing particles on the formation of SOA and BrC by the nighttime oxidation of furan, the representative structural backbone and most abundant component of furans. The oxidant levels here refer to NO_3 concentrations (hereafter denoted as “NO_3 levels”), which are controlled by the concentration ratios of nitrogen dioxide to ozone ($[NO_2]/[O_3]$), whereas the pre-existing particles in this study are ammonium sulfate particles. The compositional variation of SOA under various environmental conditions was investigated. Light-absorption properties of SOA and chromophores were characterized to determine the effects of NO_3 levels and pre-existing particles on secondary BrC formation.

METHODS

Experimental setup. All the experiments were conducted in a 10 m^3 Teflon FEP chamber under dark conditions. Details of the experimental setup and procedures were introduced in our previous studies.[31, 32] In brief, 1500 ppb O_3 and 150 ppb or 450 ppb NO_2 (i.e., initial $[NO_2]/[O_3] = 0.1$ or 0.3, denoted as "low NO_3" and "high NO_3" experiments hereafter) were first injected into the chamber to produce NO_3 radicals within 1 hour of reaction, followed by the injection of ~200 ppb furan. The stabilized NO_3 radical concentration before furan injection was estimated to be ~8.0 ppb and ~22.0 ppb under the "low NO_3" and "high NO_3" experiments, respectively.[31] For experiments with pre-existing particles (denoted as "seeded experiments" hereafter), a constant output atomizer (TSI 3076) with 10 mM ammonium sulfate ($(NH_4)_2SO_4$, Acros Organics, 99%, extra pure) solution and a silica-gel diffusion dryer were used to generate ~50 μg m^{-3} seed particles (central diameter ~50 nm) in the chamber before furan injection, simulating the background particles in wildfire plumes.[33, 34] All the experiments were performed at room temperature (20-25 °C) and low relative humidity (RH< 20%). It should be noted that when compared to real-world plumes, the chamber conditions may introduce some artifacts, such as much higher NO_3 radical concentrations than those reported by field measurements in the biomass burning plume,[35] negligible NO concentrations that may affect gas-phase organic peroxy radical (RO_2) chemistry, and wall loss of volatile products from NO_3-initiated reactions of furan. These artifacts may potentially influence the characterization of chemical composition in the experimental results.[36] Nevertheless, these controlled chamber conditions are intended to systematically investigate the role of NO_3 levels and pre-existing particles in the formation of furan-derived secondary BrC.

Compositional characterization. A combination of online and offline approaches was employed to characterize the chemical composition of furan SOA. Real-time bulk composition of aerosol particles and *in situ* molecular formula of aerosol constituents were measured online by the mini-Aerosol Mass Spectrometer coupled with a compact time-of-flight mass spectrometer (mAMS, Aerodyne Research Inc.)[37] and the iodide-adduct time-of-flight chemical ion mass spectrometry coupled with the Filter Inlet for Gases and AEROsols system (FIGAERO-ToF-CIMS, Aerodyne Research Inc.),[38] respectively. Offline techniques, including attenuated total reflectance Fourier-transform infrared spectroscopy (ATR-FTIR, Thermo Nicolet 6700), gas chromatography-electron ionization mass spectrometry (GC/EI-MS, Agilent Technologies 6890N GC System and 5975 inert XL Mass Selective Detector), liquid chromatography coupled with a diode array detector, an electrospray ionization source and a quadruple-time-of-flight mass spectrometer (LC-DAD-ESI-Q-ToFMS, Agilent Technologies 1260 Infinity II and 6545 Q-ToF LC/MS), and an ion mobility spectrometry time-of-flight mass spectrometer (IMS-TOF, Tofwerk Inc.), were used to further characterize the functional group information and molecular compositions of SOA samples. Details of the instrumental setup have been introduced in previous studies.[31, 32, 39-41]

Optical and particulate size measurements. *In situ* measurements of particulate absorption coefficients at 375 nm ($\beta_{abs,375}$) were performed by a photoacoustic extinctiometer (PAX, Droplet Measurement Technology) at 1 Hz,[42] while the ultraviolet and visible absorbance (UV-Vis) at 290-700 nm of SOA samples were measured offline by a UV-Vis spectrophotometer (Beckman DU-

640). All SOA samples were extracted with acetonitrile (ACN), a suitable solvent for secondary BrC analyses given the solubility and stability of chromophores.[32] A Scanning Electrical Mobility Spectrometer (SEMS, Brechtel Manufacturing Inc.) was used to determine the number concentration and size distribution of SOA from 10 - 800 nm with 140 bins. Online MAC at 375 nm was calculated by Eq. (1), where C_{SOA} is the mass concentration of SOA in the chamber. The offline MAC profile was calculated by Eq. (2), where $A(\lambda)$ is the absorbance along with wavelength (λ), b is the light path (i.e., 1 cm), and C_m is the mass concentration of SOA constituents in the ACN solution.

$$MAC_{online}(375) = \frac{\beta_{abs,375}}{C_{SOA}} \tag{1}$$

$$MAC_{offline}(\lambda) = \ ln10 \ \times \frac{A(\lambda)}{b \times C_m} \tag{2}$$

Absorption Ångström exponents (AAE) within 290-400 nm and 400-600 nm ($AAE_{290/400}$ and $AAE_{400/600}$) representing the wavelength dependence of light absorption in the UV and visible ranges, respectively, were calculated by the power-law dependence of offline MAC on the wavelengths (Eq. (3)).

$$AAE_{\lambda_1/\lambda_2} = \frac{-ln\left(\frac{MAC_{offline}(\lambda_1)}{MAC_{offline}(\lambda_2)}\right)}{ln\left(\frac{\lambda_1}{\lambda_2}\right)} \tag{3}$$

Particulate effective density and organic aerosol fraction of furan SOA under different environmental conditions are summarized in Table S1 for estimating C_{SOA} and C_m. Details of the instrumental setup and calculations of parameters were illustrated in our previous studies.[31, 32]

Computational details of UV-Vis spectra simulations. Time-dependent density functional theory (TD-DFT) was employed to confirm the light absorptivity of oxidation products with high double bond equivalence (DBE) identified by FIGAERO-ToF-CIMS. All the computations were performed using the Gaussian 16 program (revision C. 01).[43] Geometrical optimizations, excitation wavelengths, and oscillator strengths were computed by the B3LYP functional[44, 45] implemented with the 6-311++G(d,p) basis set,[46] which is suggested by previous studies.[47, 48] The integral equation formalism extension of the polarizable continuum model (IEFPCM)[49] was used to simulate the ACN environment. All the theoretical UV-Vis spectra were generated by the GaussView 6 program. The Cartesian coordinates for all the geometrical structures are summarized in Table S2.

RESULTS AND DISCUSSION

The role of NO_3-initiated oxidation. In order to investigate secondary BrC formation from furan, it is essential to determine whether NO_3-initiated reactions play a predominant role in furan SOA formation during the nighttime, given that O_3 concentration is significantly higher than NO_2 concentration in biomass burning plumes, where O_3 and NO_3 are likely to compete for furan oxidation.[35, 50, 51] The reaction rate constant of "furan + NO_3" ($k_{furan+NO_3}$) in the gas phase is 6 orders of magnitude greater than that of "furan + O_3" ($k_{furan+O_3}$),[52-54] indicating that NO_3-initiated reactions should account for the majority of oxidation products; the dominance of NO_3-initiated oxidation can be further verified by the method described by Draper et al.[55] (i.e.,$[NO_2]/[furan] > k_{furan+O_3}/k_{O_3+NO_2}$). Here, iodide-adduct CIMS was used to measure the gas-phase oxidation products. The O_3-only experiments (~1500 ppb O_3 as the oxidant) were implemented as a NO_x-free benchmark for comparison. Fig. 1 shows the comparison of gas-phase products under low NO_3 and O_3-only conditions, where the *m/z* 200-250 range reveals nearly identical oxidation products under both conditions, whereas the *m/z* 250-310 range reveals products that are completely dissimilar. In the presence of NO_2, despite the concentration of NO_2 being much lower than that of O_3, only nitrogen-containing products were detected in the *m/z* 250-310 range, indicating that NO_3-initiated oxidation significantly altered the reaction pathways. Moreover, as the NO_3 levels increased, the mass spectra of gas-phase products remained relatively unchanged but the intensity-weighted average values of the oxygen-to-carbon and nitrogen-to-carbon ratios (i.e., <O/C> and <N/C>) increased (Fig. S2), implying that NO_3 levels may have minimal effects on changing the molecular composition of oxygenated products but lead to a greater amount of oxidation products.

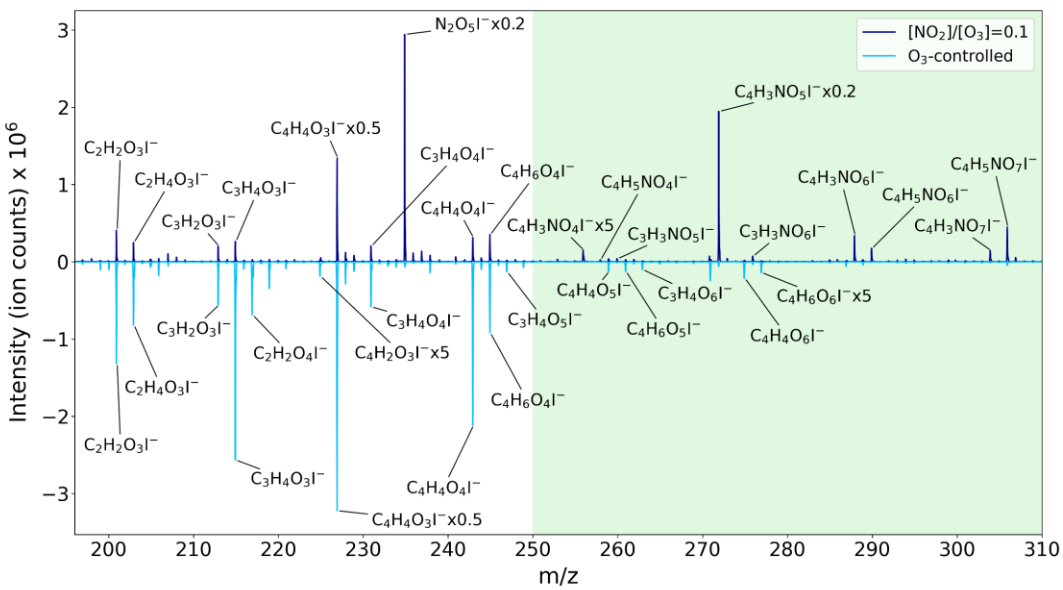

Figure 1. Comparison of gas-phase products from nighttime oxidation of furan between the low-NO_3 and O_3-only experiments. The green area highlights the compositional difference under the two environmental conditions.

Gas-phase products can contribute to SOA formation via new particle formation or gas-particle partitioning on aerosols, where heterogeneous and multiphase chemistry (e.g., reactive uptake of gaseous oxidants onto aerosols) can promote further reactions and thus generate a wider array of secondary products. However, since the mechanistic understanding of NO_3-initiated oxidation of furan is still lacking, process-level insights into SOA formation in this case are very limited. Berndt et al.[56] and Zhang et al.[57] reported the formation mechanisms of 3H-furan-2-one and dicarbonyls (e.g., *cis*-butenedial) initiated by NO_3 addition on the furan ring, whereas Jiang et al.[21] recently proposed a mechanistic scheme of NO_3-initiated reactions with furan. Nonetheless, little understanding of oxidation products has been experimentally supported thus far. In this study, Fig. 1 may suggest the generation of 2-peroxyl-5-nitrate-furan ($C_4H_5NO_6$), 5-nitrate-furan-2-one ($C_4H_3NO_5$, the highest peak in the upper panel) and formyl nitrate methyl formylate ($C_3H_3NO_6$) in the mechanisms proposed by Jiang et al.[21] In addition, nitrate-furan ($C_4H_3NO_4$) was detected here, which is consistent with our previous findings.[28] Furthermore, our data could support field observations. For example, Palm et al.[14] proposed that furan oxidation may contribute to $C_4H_4O_4$ and $C_3H_4O_4$ observed in the biomass burning plume, which can be supported by Fig. 1.

While the characterization of gas-phase products reveals the remarkable alteration of oxidation pathways in the presence of NO_2, SEMS measurements highlight the effect of NO_3-initiated reactions on SOA formation kinetics. As soon as furan was injected into the chamber where NO_2 and O_3 had been reacting for 1 h, SOA was formed immediately (Fig. 2A and 2C). In the O_3-only experiments, no particles were generated within ~30 min after furan injection (Fig. 2E). As seed particles were added, instant generation of SOA occurred after furan injection (Fig. 2B and 2D), whereas no rapid formation of SOA was observed in O_3-only, seeded experiments (Fig. 2F). These results demonstrate the advantage of NO_3-initiated reactions in rapidly producing low volatile products and thus accelerating SOA formation, and consequently, NO_3-initiated oxidation should account for the majority of furan SOA in nighttime biomass burning plumes.

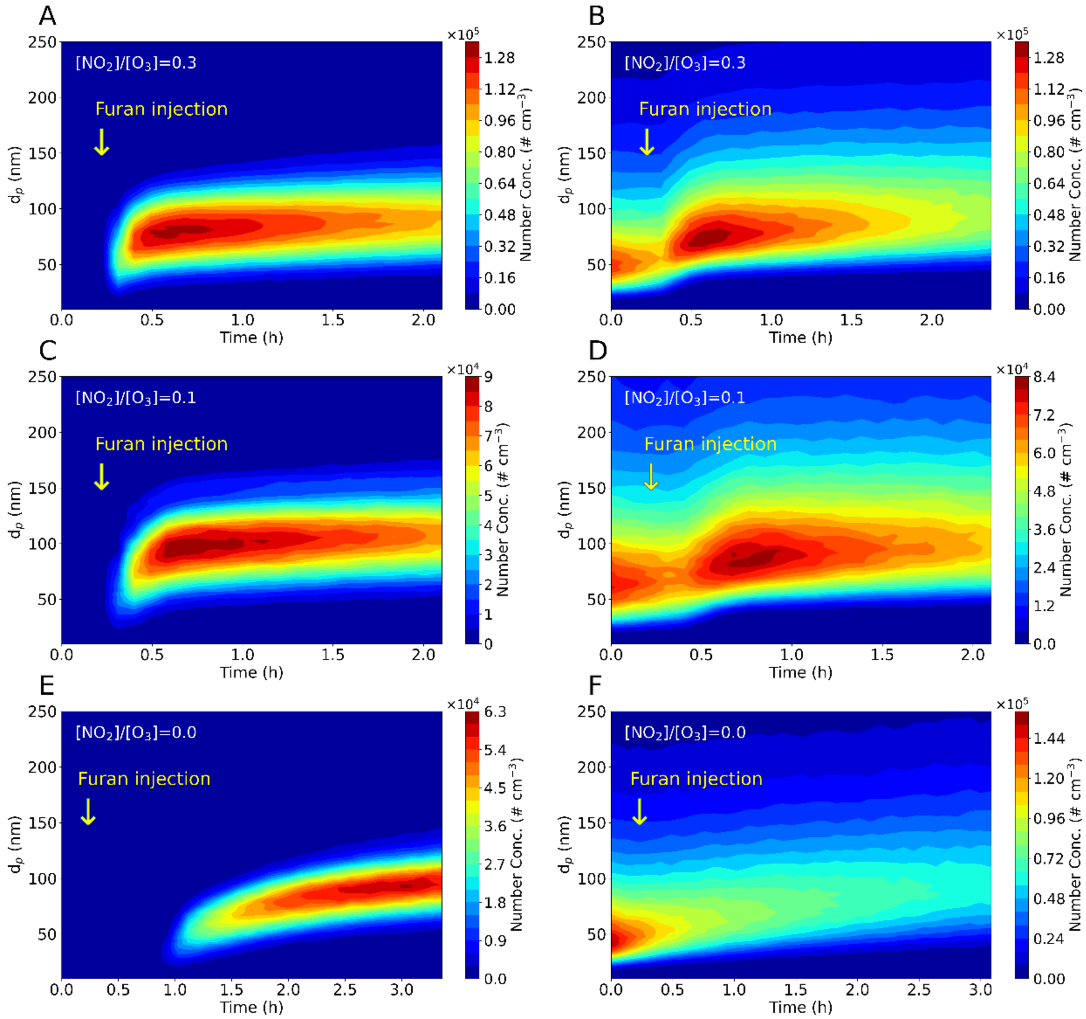

Figure 2. Size and number distribution of furan SOA along with the experimental time. Experimental conditions: (A) $[NO_2]/[O_3]$ = 0.3, non-seeded, (B) $[NO_2]/[O_3]$ = 0.3, seeded, (C) $[NO_2]/[O_3]$ = 0.1, non-seeded, (D) $[NO_2]/[O_3]$ = 0.1, seeded, (E) O_3-only, non-seeded, (F) O_3-only, seeded.

SOA constituents under various environmental conditions. Fig. 3 depicts the characterization of SOA in bulk composition and at the molecular level measured by mAMS and FIGAERO-ToF-CIMS, respectively. In this study, pie charts were used to visualize the average relative abundance of $C_xH_y^+$, $C_xH_yO^+$, $C_xH_yO_{>1}^+$, $C_xH_yN^+$, and $C_xH_yNO^+$ fractions during the experiments. To show the change in relative abundance of fraction signals during the experiments, the average value of each fraction was calculated at (1) 20-30 minutes and (2) 95-115 minutes after the injection of furan. These time intervals were selected to represent the early and late stages of the experiment, and the corresponding averages are named as "early averages" and "late averages" (Fig. S1). The comparison of these two timeframes allows differentiation between mechanisms of particle formation; the "early average" represents the nucleation of atmospheric particles, whereas the "late average" represents the condensation of oxidation products on already formed SOA. Fig. S1 reveals that the two mechanisms may result in overall similar chemical compositions, meaning that the SOA generated from the nucleation in the non-seeded experiments may have on average a comparable composition to those formed from the condensation process. The condensation process is expected to be more atmospherically relevant due to the abundance of pre-existing particles in the biomass burning plume. The relative abundance of investigated fragments ($C_xH_y^+$, $C_xH_yO^+$, $C_xH_yO_{>1}^+$, $C_xH_yN^+$ and $C_xH_yNO^+$) is roughly consistent among all of the experimental conditions, where $C_xH_yO^+$ and $C_xH_yO_{>1}^+$ fragments contribute to ~60-70% and $C_xH_yN^+$ plus $C_xH_yNO^+$ contribute to ~8-13%, suggesting the dominance of $C_xH_yO_z$-containing products and a considerable amount of nitrogen-containing products in furan SOA.

In addition, the ratio of NO^+/NO_2^+ in all experiments was higher than what is expected from inorganic nitrates (1.30-1.42)[58, 59] (Table S3), confirming that some of the measured nitrate by the mAMS was organic in nature. However, the ratio did not show significant changes with oxidation time, suggesting that the contribution of the organic portion of nitrate to total nitrate did not change with the extent of oxidation. More importantly, higher NO_3 conditions did not result in significantly higher NO^+/NO_2^+ ratios for non-seeded experiments, suggesting again that the fraction of organonitrates/nitro-organic species in total nitrate was independent of the NO_3 concentration. In contrast, seeded, high NO_3 experiments displayed higher ratios of NO^+/NO_2^+ compared to seeded, low NO_3 experiments, indicating that higher NO_3 levels had resulted in a higher fraction of organonitrate/nitro-organics in the aerosols instead of inorganic nitrate. Regardless of NO_3 levels, the presence of seed decreased the contribution of organonitrate/nitro organics since significantly lower NO^+/NO_2^+ were observed in seeded experiments compared to non-seeded ones.

The molecular compositions of SOA constituents shown in Fig. 3 highlight the C_4 and C_8 products, which represent the monomer and dimer products of furan oxidation. In the non-seeded experiments, $C_4H_2O_4$ is the highest peak (Fig. 3A-B), but in the seeded experiments, the intensity of $C_4H_4O_3$ is comparable to $C_4H_2O_4$ (Fig. 3C) or even exceeds $C_4H_2O_4$ (Fig. 3D). Since $C_4H_4O_3$ is also detected in the gas phase (Fig. 1 and Fig. S2), the $C_4H_4O_3$ found in the aerosol phase should be attributed to gas-particle partitioning facilitated by pre-existing particles. However, $C_4H_2O_4$ is not observed in the gas-phase mass spectra, suggesting that rapid gas-particle partitioning and/or condensed-phase reactions on aerosols may contribute to this product. Notably, $C_4H_2O_5$, a more oxidized formula compared to $C_4H_2O_4$, is only detected in seeded experiments, implying that pre-existing particles may facilitate the generation of further oxidation products. Incremental addition of oxygen in other C_4 monomer series (i.e., $C_4H_4O_3$, $C_4H_4O_4$ and $C_4H_4O_5$; $C_4H_6O_4$ and $C_4H_6O_5$) is also observed in all the panels of Fig. 3, indicating common pathways of $C_xH_yO_z$ product formation in furan SOA under all the environmental conditions. In addition, a series of dimers were identified in furan SOA (Fig. 3). $C_8H_4O_3$ is most likely phthalic anhydride, which has been confirmed previously as a chromophore in secondary furan BrC,[32] while $C_8H_3NO_5$ could be its nitro-substituted product. Furthermore, IMS-TOF characterization of SOA constituents show significant differences in isomer distribution of oxygenated products led by the pre-existing particles while similar isomer distribution under the "high NO_3" and "low NO_3" conditions (Fig. S3), revealing that pre-existing particles can alter the reaction pathways and hence modify SOA constituents.

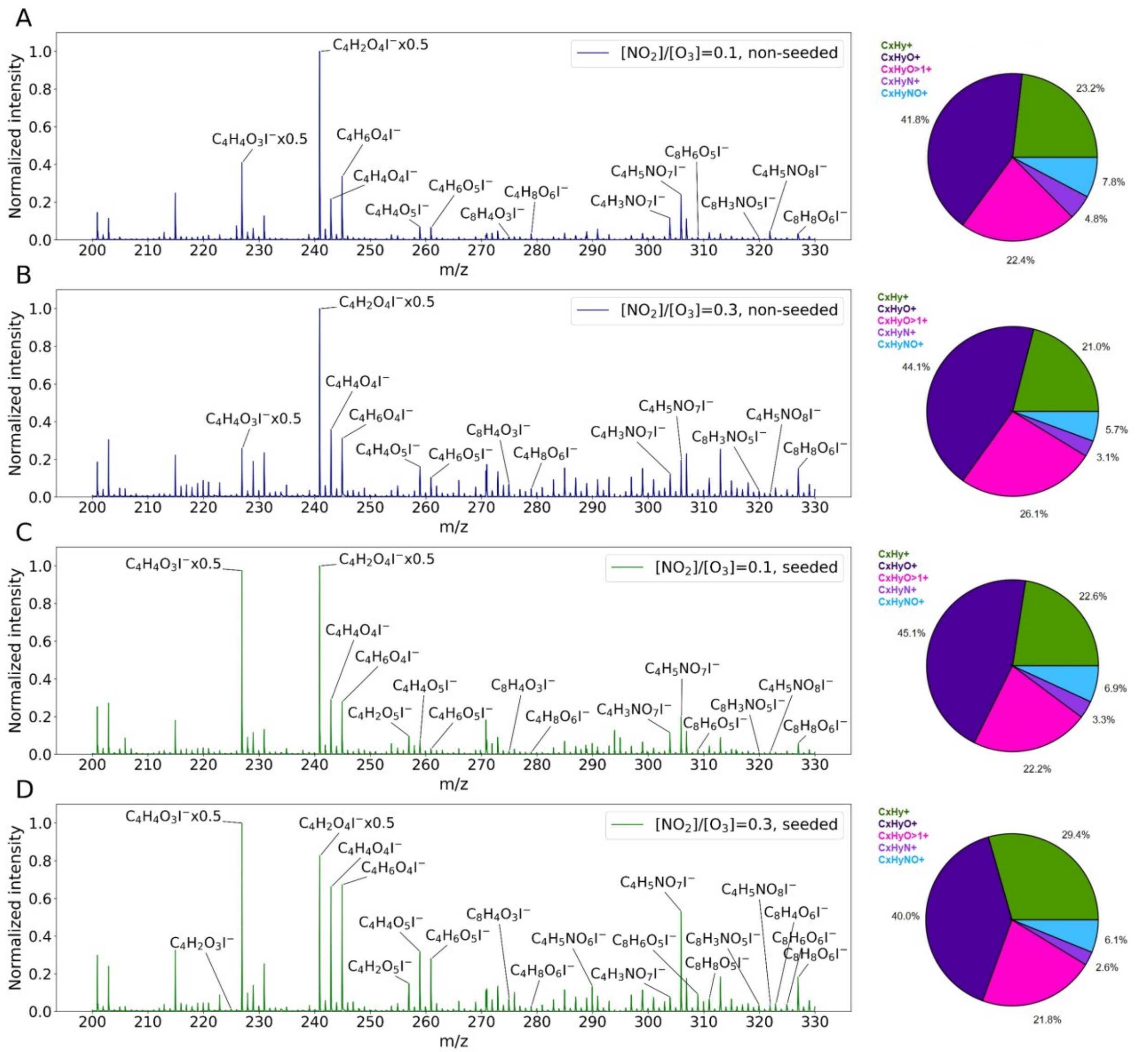

Figure 3. Molecular compositions of SOA measured by FIGAERO-ToF-CIMS and bulk compositions of SOA measured as ion fragment families by mAMS under various experimental conditions. (A) $[NO_2]/[O_3]$ = 0.1, non-seeded; (B) $[NO_2]/[O_3]$ = 0.3, non-seeded; (C) $[NO_2]/[O_3]$ = 0.1, seeded; (D) $[NO_2]/[O_3]$ = 0.3, seeded. Pie charts show the relative abundance of the investigated fragments: $C_xH_y^+$, $C_xH_yO^+$, $C_xH_yO_{>1}^+$, $C_xH_yN^+$ and $C_xH_yNO^+$.

Fingerprints of functional groups characterized by the ATR-FTIR can also provide further evidence to reveal the divergence of SOA constituents under various environmental conditions. Fig. 4 highlights three wavenumber regions that illustrate the compositional difference. The orange area shades the wavenumber 1600-1800 cm^{-1}, which corresponds to the stretching modes of carbonyl groups (>C=O). Two peaks are seen at 1643 cm^{-1} and 1730 cm^{-1}, respectively; the first can also be attributed to the stretching of aliphatic C=C double bonds, but the latter is attributable only to >C=O stretching.[60] Without pre-existing particles, the presence of NO_2 flattens the peak at 1643 cm^{-1} but raises the peak at 1730 cm^{-1} (Fig. 4A), which may be attributed to the higher consumption of aliphatic C=C double bonds along with the enhanced generation of carbonyl products during NO_3-initiated oxidation. This could be due to the fact that the NO_3-initiated oxidation of furan is much faster than the O_3-initiated oxidation,[52-54] and the "addition-elimination mechanism," in which carbonyls are produced along with the loss of NO_2 from the NO_3 groups added to furan, is the most energetically favorable pathway in the NO_3-initiated oxidation of furan.[57] However, the presence of pre-existing particles inhibits the peak at 1730 cm^{-1} (Fig. 4B), implying further reactions of carbonyl products on the seed particles. The blue-shaded area (1300-1500 cm^{-1}) represents a mixture of functional group signals, with the O_3-only experiment producing three sharp peaks in the absence of seeds, while both NO_3 conditions produce only one peak at 1360 cm^{-1} (Fig. 4A). This occurrence suggests that the presence of NO_2 together with O_3 can significantly modify the SOA compositions, but SOA compositions are insensitive to the changes in NO_3 levels. In contrast, only broad peaks were observed in seeded experiments (Fig. 4B), highlighting the role of pre-existing particles in modifying the SOA constituents. The green-shaded area has a strong peak at 1095 cm^{-1} (i.e., C-O-C stretching[61]) in the seeded experiments, which may be attributed to the gas-particle partitioning of more volatile oxidation products that preserve the furan backbone facilitated by pre-existing particles.

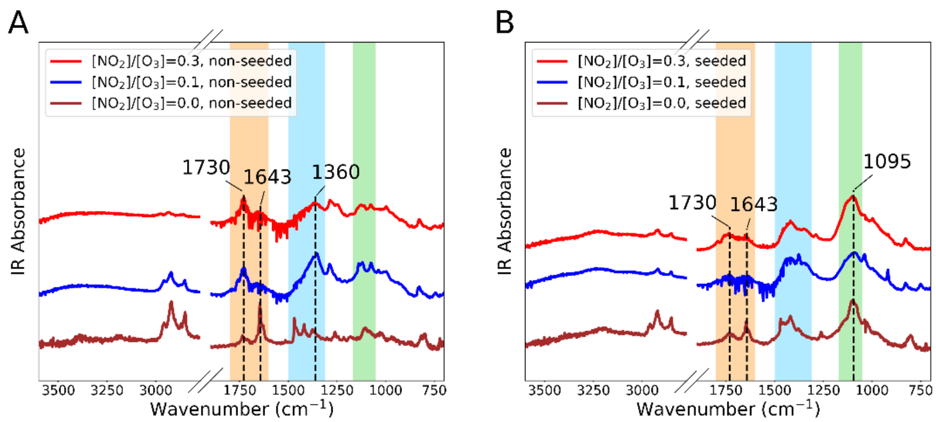

Figure 4. ATR-FTIR spectra corresponding to the ACN-extracted aerosol samples from nighttime oxidation of furan under different environmental conditions.

In addition, the formation of organosulfur products was observed in the presence of pre-existing particles (Fig. S4), which indicates the unique condensed-phase chemistry supported by the sulfate-containing pre-existing particles (i.e., $(NH_4)_2SO_4$). Overall, the compositional profiles of furan-derived SOA may be resistant to the changes in NO_3 levels, but they can vary in the presence of pre-existing particles.

Light-absorption properties of furan BrC. The wavelength dependent MACs are depicted in Fig. 5. The SOA mass concentration and online MAC at 375 nm (MAC_{375}) are provided in Table 1, followed by the $AAE_{290/400}$ and $AAE_{400/600}$. Fig. 5 shows the elevated MACs related to the increased NO_3 levels. Given the consistent SOA mass concentrations under the various NO_3 levels studied (Table 1), our findings indicate that higher levels of NO_3-initiated oxidation can result in the production of more BrC constituents absorbing in the near UV range. Furthermore, the presence of pre-existing particles led to higher the SOA mass concentrations (Table 1) and lower MAC profiles (Fig. 5). Because pre-existing particles can facilitate gas-particle partitioning and promote SOA formation by enhancing aerosol-phase reactions, it appears that the seed promoted the addition of non-absorbing products more compared to BrC chromophores. Our results may also suggest that semi-volatile products that would not condense without the seed are not as light-absorbing compared to the low-volatile products that condense under both conditions. To rule out potential interference caused by solvent effects during extractions,[32] online MAC_{375} measurements were also compared. The results show the consistency of MAC_{375} under the studied NO_3 levels but a reduction by half of MAC_{375} in the presence of pre-existing particles (Table 1). In addition, the results of $AAE_{290/400}$ and $AAE_{400/600}$ may indicate that MAC profiles have a weaker wavelength dependence of in the presence of pre-existing particles.

Moreover, Fig. 6 shows the LC-DAD chromatograms (absorption wavelength versus the chromatographic retention time), where each heatmap displays the relative light absorption intensity of chromophores under the corresponding experimental conditions. All the chromophores are distributed in the UV range, agreeing with the MAC profiles (Fig. 5), in which the major absorption is below 400 nm. The distribution of chromophores exhibits a similar pattern in the LC-DAD chromatogram for all the experimental conditions, where the strongest light absorption hotspot emerges within the retention time between 1.5-2.0 min, while several weaker absorption hotspots are spread over 7.0-17.0 min. Moreover, the strongest hotspot has the highest absorption at ~300 nm, while those weaker hotspots are spread within the range of 300-400 nm, corresponding to the protruding shoulder at ~350 nm in the MAC profiles (Fig. 5).

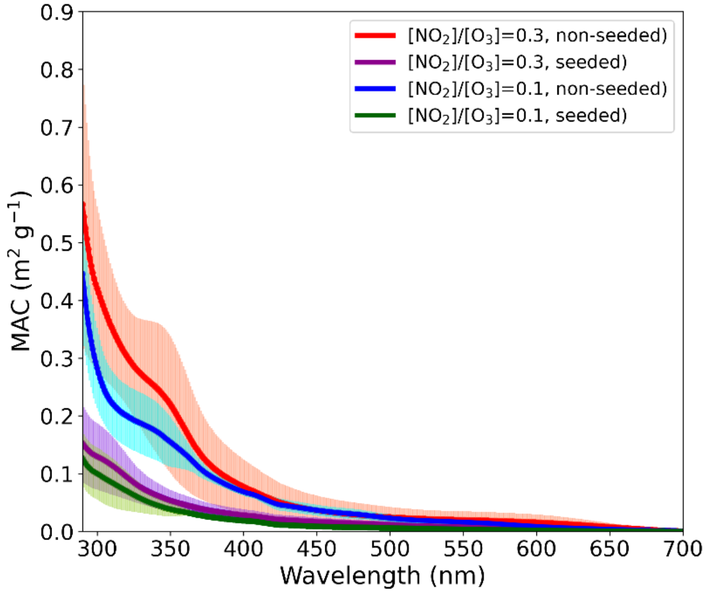

Figure 5. MAC profiles of furan BrC under the investigated conditions. The spectral curves are estimated by the average of three replica samples and the shared areas are estimated by the corresponding standard deviations of MAC at each wavelength.

Table 1. Summary of C_{SOA}, online MAC_{375}, $AAE_{290/400}$ and $AAE_{400/600}$ under different environmental conditions. Results are expressed as mean ± 1 standard deviation (SD) from triplicate experiments. The data shown in the non-seeded experiments were from our previous study.[32]

$[NO_2]/[O_3]$	Pre-existing particles	C_{SOA} (μg m^{-3})	MAC_{375} (m^2 g^{-1})	$AAE_{290/400}$	$AAE_{400/600}$
0.1	No	17.73 ± 1.68	0.09 ± 0.03	5.82 ± 0.55	5.28 ± 0.85
	Yes	42.46 ± 1.80	0.04 ± 0.01	3.26 ± 1.36	3.98 ± 0.65
0.3	No	17.74 ± 1.65	0.08 ± 0.01	5.98 ± 1.03	4.14 ± 0.30
	Yes	40.86 ± 5.15	0.04 ± 0.01	4.11 ± 0.88	3.93 ± 0.84

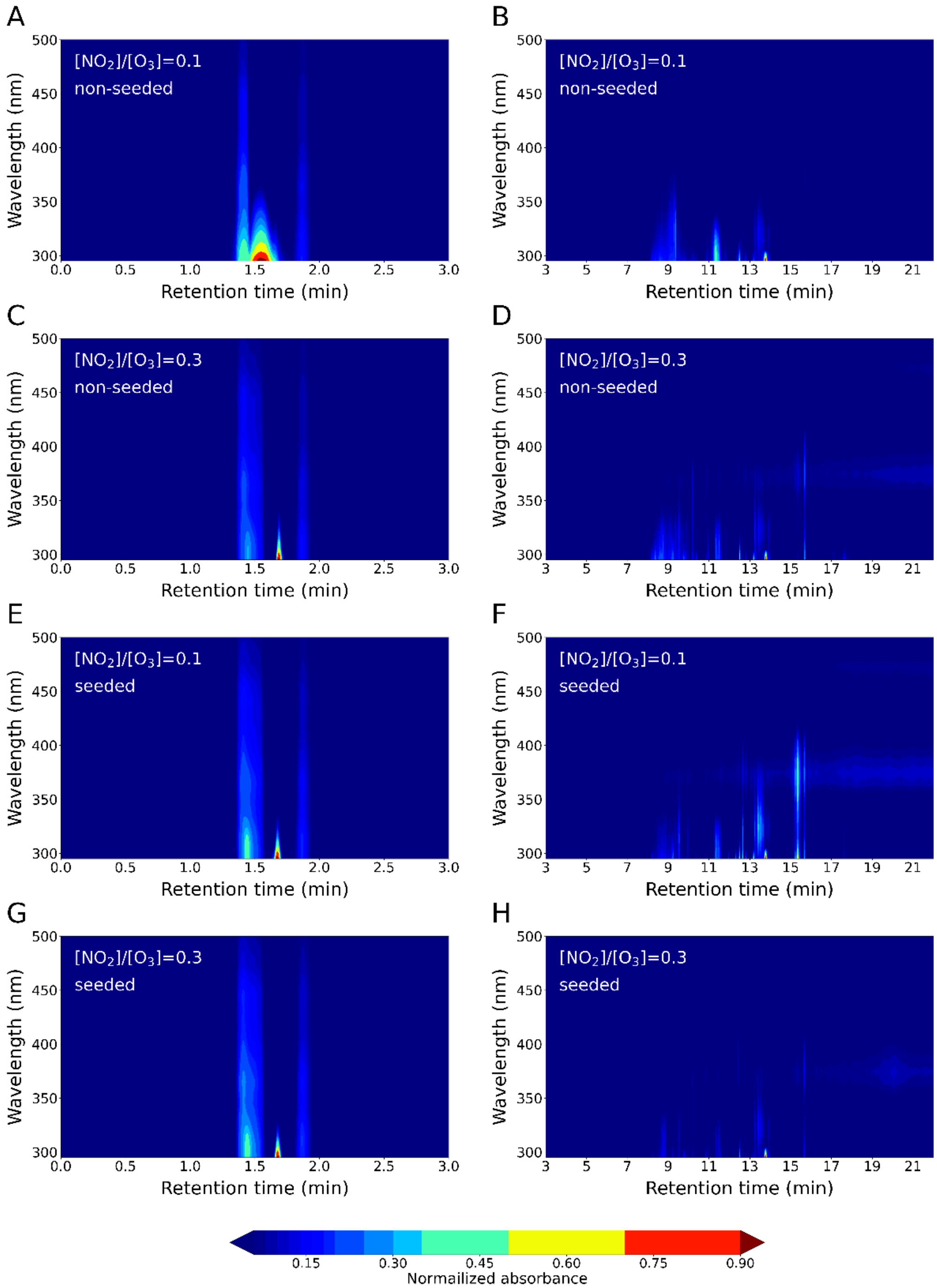

Figure 6. LC-DAD heatmap of furan BrC chromophores under various environmental conditions.

Molecular compositions of chromophores in furan BrC

Understanding the chromophore composition is fundamental to the process-level evaluation of secondary BrC formation. Since the strongest absorption hotspot in Fig. 6 is at around

1.7 min and 290 nm, the DAD chromatogram at 290 nm is extracted (Fig. 7A) and the mass spectrum of the identified peak is analyzed (Fig. 7B). The predominant peak in the mass spectrum is assigned to the deprotonated anion (i.e., $[M-H]^-$) of $C_4H_4O_6$, whose extracted ion chromatogram (EIC) also shows a distinct peak at 1.7 min (Fig. 7C). $C_4H_4O_6$ is a highly oxidized product and could be generated from further oxidation of $C_4H_4O_3$, $C_4H_4O_4$ and $C_4H_4O_5$ that were identified in the FIGAERO-CIMS data (Fig. 3). The measured UV-Vis spectrum from LC-DAD shows a similar sketch to the MAC profiles (Fig. 5), indicating that $C_4H_4O_6$ is one of the major chromophores in furan BrC from nighttime oxidation (Fig. 6).

As discussed above, the hotspots over 7.0-17.0 min from LC-DAD can contribute to the protruding shoulder in the MAC profiles (Fig. 5). Compositional analysis reveals that these hotspots may be attributable to higher molecular weight oxidation products (i.e., dimers and oligomers) with high double bond equivalents (DBE). For example, Fig. S5A-C shows three dimers, $C_8H_6O_4$ (DBE = 6), $C_8H_6O_6$ (DBE = 6) and $C_8H_4O_6$ (DBE = 7), which may correlate to the hotspots at 9 min and 11.2 min, respectively. The oligomers $C_{14}H_{22}O_5$ (DBE = 4), $C_{15}H_{21}NO_5$ (DBE = 5) and $C_{10}H_{13}NO_5$ (DBE = 4) shown in Fig. S5D-F may correspond to the hotspots at 11.2 min and 13.5 min, respectively. Notably, because each hotspot shown in the heatmap may account for multiple chromophores (e.g., Fig. S5B-E), it is challenging to quantify their contributions here without authentic standards. Nevertheless, dimers and oligomers appear to play an important role in BrC light absorption in furan SOA.

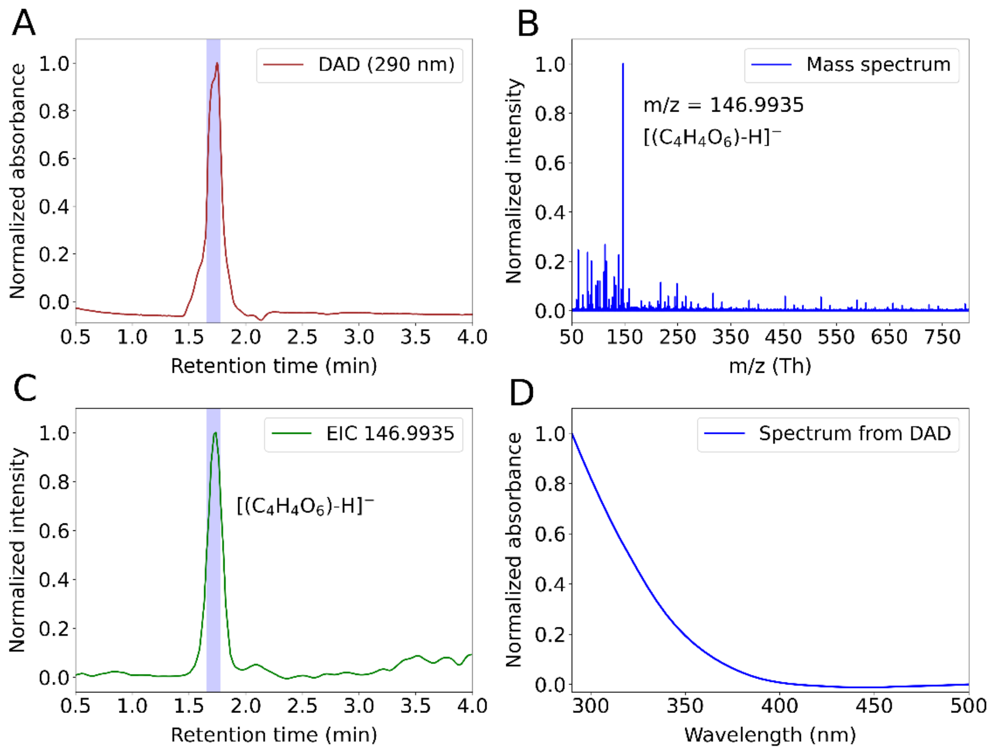

Figure 7. Identification of $C_4H_4O_6$ as a BrC chromophore. (A) DAD extracted wavelength chromatogram at 290 nm, (B) extracted mass spectrum of the shaded area in the DAD chromatogram, (C) EIC of the deprotonated $C_4H_4O_6$, and (D) UV-Vis spectrum from the shaded area in the DAD chromatogram.

Due to the smaller proportion of nitrogen-containing products in furan SOA compositions, the solvent selectivity or artifacts during LC analysis that may further impede the detection of chromophores that are sensitive to solvent attacks (e.g., hydrolysis or methanolysis of anhydrides by LC mobile phases).[32] In addition, not all the SOA components can be efficiently ionized by the ESI source.[62, 63] As a result, identified chromophores in this subset by LC-DAD-ESI-Q-ToFMS are limited. However, several unsaturated nitrogen-containing products were identified by an independent solvent-free approach using FIGAERO-ToF-CIMS; thus, we performed TD-DFT calculations to determine whether these products could be potential chromophores. For instance, $C_4H_3NO_7$ (DBE = 3), is a functionalized monomer which may have two light-absorbing isomers:

2-hydroxy-3-nitro-maleic acid and 2-hydroxy-3-nitro-fumaric acid (Fig. 8A). $C_8H_3NO_5$ (DBE = 7) is likely nitrophthalic anhydrides that are susceptible to solvent attacks (Fig. 8B). Given the strong absorptivity of these products, nitrogen-containing chromophores may still contribute significantly to BrC light absorption even though their mass fraction is small.

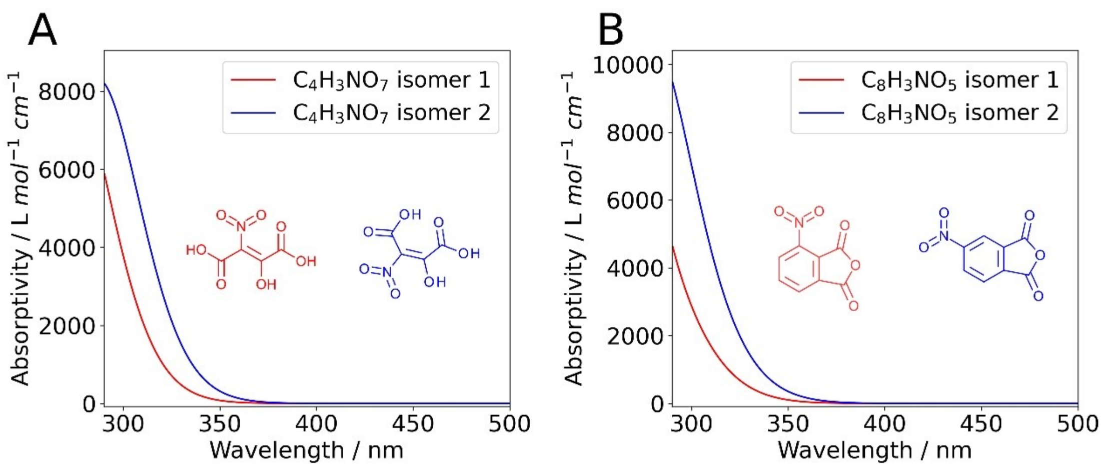

Figure 8. Theoretical UV-Vis spectra of nitrogen-containing chromophores: (A) $C_4H_3NO_7$ and (B) $C_8H_3NO_5$.

Atmospheric implications

This study investigated the secondary BrC formation from nighttime oxidation of furan by varying the NO_3 levels and pre-existing particles. Our analysis revealed the key role of NO_3-initiated oxidation in furan oxidation under the in-plume environment and highlighted the effects of oxidant levels and pre-existing particles on chemical compositions and optical properties. Increased NO_3 levels can enhance the MAC profiles, but the overall bulk compositions in furan SOA measured as ion fragment families by mAMS are insensitive to this change. Since rapid SOA formation has been observed in biomass burning plumes exposed to NO_2 and O_3 during the nighttime but has not been well represented in modeling studies,[64] our work contributes to a better understanding of the role of nighttime oxidant levels in furan SOA formation and BrC light absorption. Our results also indicate that the pre-existing particles can increase the SOA mass concentrations but, in the meantime, decrease the MAC profiles under dry conditions (RH< 20%). MAC reduction due to pre-existing particles under dry conditions may be an important process for evaluating BrC radiative forcing in climate models, as pre-existing particles have been demonstrated as a crucial factor that controls SOA formation in a changing climate.[65]

Our study is pertinent to biomass burning plumes with low RH (e.g., the Williams Fire plume[66]) or plumes of higher RH expanded into the low RH atmospheres, such as those in the western United States[67, 68] and Africa during dry seasons.[69, 70] The molecular compositions reported here can contribute to a more comprehensive molecular understanding of furan oxidation. We show that under different environmental conditions, highly oxidized monomers, dimers, and oligomers can contribute to BrC chromophores. Multiple anhydride species, including maleic anhydride (or furandione), phthalic anhydride, and nitrophthalic anhydrides, can be potentially important chromophores in furan BrC under dry conditions.[32] Notably, atmospheric convection can vertically transport BrC into the upper troposphere,[71] where the average relative humidity is approximately 27% and less than 10% for subtropical regions.[72] Anhydride chromophores are likely to have a longer lifetime in the upper troposphere. Even under wet conditions where anhydrides could be hydrolyzed, the resulting products may still be chromophores. For example, phthalic acid (or 1,2-benzenedicarboxylic acid), the hydrolysis product of phthalic anhydride, has been reported as one of the most prevalent BrC chromophores in ambient observations.[73, 74] Nitrophthalic acid, the hydrolysis product of nitrophthalic anhydrides, was also identified as a chromophore in the aerosols produced by the combustion of biomass.[75] Since both of these hydrolysis products are organic markers of SOA,[76-79] the hydrolysis of anhydrides can be used to track the formation and evolution of secondary BrC. Overall, our findings highlight the influence of NO_3 levels and pre-existing particles on the chemical composition and optical properties of nighttime furan SOA, whereas bulk and molecular characterizations of SOA constituents and chromophores are necessary for better experimental constraint and a more complete process-level understanding of their formation.

AUTHOR INFORMATION

Supporting Information

Pie charts for the early averages and the late averages of fragments (Figure S1); gas-phase products under the "low NO_3" and "high NO_3" conditions (Figure S2); IMS-TOF characterizations of oxidation products (Figure S3); EICs of organosulfur products (Figure S4); EICs of light-absorbing dimers and oligomers (Figure S5); summary of particulate effective density and organic aerosol fraction (Table S1); Cartesian coordinates for geometrical structures in the theoretical calculations (Table S2); summary of NO^+/NO_2^+ ratio (Table S3).

Corresponding Author

* Phone: +1-951-827-3785. E-mail: ying-hsuan.lin@ucr.edu

Notes

The authors declare no competing financial interest.

ACKNOWLEDGEMENT

This work was supported by NSF AGS-1953905 and the UCR Hellman Fellowship granted to Ying-Hsuan Lin. We thank Dr. Lingchao Zhu and Dr. Jie Zhou at UCR Analytical Chemistry Instrumentation Facility (ACIF) for their assistance with Thermo Nicolet 6700 ATR-FTIR (supported by UCR Chemistry ACIF Fund) and UPLC-DAD-ESI-Q-TOFMS (supported by NSF

CHE-0541848). We gratefully acknowledge use of the PAX instrument acquired with support from NSF AGS-1454374. We would like to thank Yumeng Cui at UCR Department of Environmental Sciences for assisting with the instrumental operation during the experiments.

REFERENCE

1. Ma, Y.; Hays, M. D., Thermal extraction–two-dimensional gas chromatography–mass spectrometry with heart-cutting for nitrogen heterocyclics in biomass burning aerosols. *J. Chromatogr. A* **2008,** *1200*, (2), 228-234.
2. Akagi, S. K.; Yokelson, R. J.; Burling, I. R.; Meinardi, S.; Simpson, I.; Blake, D. R.; McMeeking, G. R.; Sullivan, A.; Lee, T.; Kreidenweis, S.; Urbanski, S.; Reardon, J.; Griffith, D. W. T.; Johnson, T. J.; Weise, D. R., Measurements of reactive trace gases and variable O3 formation rates in some South Carolina biomass burning plumes. *Atmos. Chem. Phys.* **2013,** *13*, (3), 1141-1165.
3. Hatch, L. E.; Luo, W.; Pankow, J. F.; Yokelson, R. J.; Stockwell, C. E.; Barsanti, K. C., Identification and quantification of gaseous organic compounds emitted from biomass burning using two-dimensional gas chromatography–time-of-flight mass spectrometry. *Atmos. Chem. Phys.* **2015,** *15*, (4), 1865-1899.
4. Stefanova, M.; Marinov, S. P.; Mastral, A. M.; Callén, M. S.; Garcí, T., Emission of oxygen, sulphur and nitrogen containing heterocyclic polyaromatic compounds from lignite combustion. *Fuel Process. Technol.* **2002,** *77-78*, 89-94.
5. Liang, F.; Lu, M.; Birch, M. E.; Keener, T. C.; Liu, Z., Determination of polycyclic aromatic sulfur heterocycles in diesel particulate matter and diesel fuel by gas chromatography with atomic emission detection. *J. Chromatogr. A* **2006,** *1114*, (1), 145-153.
6. Westerling, A. L.; Hidalgo, H. G.; Cayan, D. R.; Swetnam, T. W., Warming and Earlier Spring Increase Western U.S. Forest Wildfire Activity. *Science* **2006,** *313*, (5789), 940-943.
7. Shi, G.; Yan, H.; Zhang, W.; Dodson, J.; Heijnis, H.; Burrows, M., Rapid warming has resulted in more wildfires in northeastern Australia. *Sci. Total Environ.* **2021,** *771*, 144888.
8. Baker, S. J., Fossil evidence that increased wildfire activity occurs in tandem with periods of global warming in Earth's past. *Earth Sci. Rev.* **2022,** *224*, 103871.
9. Mettler, M. S.; Mushrif, S. H.; Paulsen, A. D.; Javadekar, A. D.; Vlachos, D. G.; Dauenhauer, P. J., Revealing pyrolysis chemistry for biofuels production: Conversion of cellulose to furans and small oxygenates. *Energy Environ. Sci.* **2012,** *5*, (1), 5414-5424.
10. Koss, A. R.; Sekimoto, K.; Gilman, J. B.; Selimovic, V.; Coggon, M. M.; Zarzana, K. J.; Yuan, B.; Lerner, B. M.; Brown, S. S.; Jimenez, J. L.; Krechmer, J.; Roberts, J. M.; Warneke, C.; Yokelson, R. J.; de Gouw, J., Non-methane organic gas emissions from biomass burning: identification, quantification, and emission factors from PTR-ToF during the FIREX 2016 laboratory experiment. *Atmos. Chem. Phys.* **2018,** *18*, (5), 3299-3319.
11. Sekimoto, K.; Koss, A. R.; Gilman, J. B.; Selimovic, V.; Coggon, M. M.; Zarzana, K. J.; Yuan, B.; Lerner, B. M.; Brown, S. S.; Warneke, C.; Yokelson, R. J.; Roberts, J. M.; de Gouw, J., High- and low-temperature pyrolysis profiles describe volatile organic compound emissions from

western US wildfire fuels. *Atmos. Chem. Phys.* **2018,** *18*, (13), 9263-9281.

12. Ahern, A. T.; Robinson, E. S.; Tkacik, D. S.; Saleh, R.; Hatch, L. E.; Barsanti, K. C.; Stockwell, C. E.; Yokelson, R. J.; Presto, A. A.; Robinson, A. L.; Sullivan, R. C.; Donahue, N. M., Production of Secondary Organic Aerosol During Aging of Biomass Burning Smoke From Fresh Fuels and Its Relationship to VOC Precursors. *J. Geophys. Res. Atmos.* **2019,** *124*, (6), 3583-3606.

13. Gilman, J. B.; Lerner, B. M.; Kuster, W. C.; Goldan, P. D.; Warneke, C.; Veres, P. R.; Roberts, J. M.; de Gouw, J. A.; Burling, I. R.; Yokelson, R. J., Biomass burning emissions and potential air quality impacts of volatile organic compounds and other trace gases from fuels common in the US. *Atmos. Chem. Phys.* **2015,** *15*, (24), 13915-13938.

14. Palm, B. B.; Peng, Q.; Fredrickson, C. D.; Lee, B. H.; Garofalo, L. A.; Pothier, M. A.; Kreidenweis, S. M.; Farmer, D. K.; Pokhrel, R. P.; Shen, Y.; Murphy, S. M.; Permar, W.; Hu, L.; Campos, T. L.; Hall, S. R.; Ullmann, K.; Zhang, X.; Flocke, F.; Fischer, E. V.; Thornton, J. A., Quantification of organic aerosol and brown carbon evolution in fresh wildfire plumes. *PNAS* **2020,** *117*, (47), 29469.

15. Atkinson, R.; Aschmann, S. M.; Tuazon, E. C.; Arey, J.; Zielinska, B., Formation of 3-Methylfuran from the gas-phase reaction of OH radicals with isoprene and the rate constant for its reaction with the OH radical. *Int. J. Chem. Kinet.* **1989,** *21*, (7), 593-604.

16. Sprengnether, M.; Demerjian, K. L.; Donahue, N. M.; Anderson, J. G., Product analysis of the OH oxidation of isoprene and 1,3-butadiene in the presence of NO. *J. Geophys. Res. Atmos.* **2002,** *107*, (D15), ACH 8-1-ACH 8-13.

17. Francisco-Márquez, M.; Alvarez-Idaboy, J. R.; Galano, A.; Vivier-Bunge, A., A Possible Mechanism for Furan Formation in the Tropospheric Oxidation of Dienes. *Environ. Sci. Technol.* **2005,** *39*, (22), 8797-8802.

18. Stefenelli, G.; Jiang, J.; Bertrand, A.; Bruns, E. A.; Pieber, S. M.; Baltensperger, U.; Marchand, N.; Aksoyoglu, S.; Prévôt, A. S. H.; Slowik, J. G.; El Haddad, I., Secondary organic aerosol formation from smoldering and flaming combustion of biomass: a box model parametrization based on volatility basis set. *Atmos. Chem. Phys.* **2019,** *19*, (17), 11461-11484.

19. Akherati, A.; He, Y.; Coggon, M. M.; Koss, A. R.; Hodshire, A. L.; Sekimoto, K.; Warneke, C.; de Gouw, J.; Yee, L.; Seinfeld, J. H.; Onasch, T. B.; Herndon, S. C.; Knighton, W. B.; Cappa, C. D.; Kleeman, M. J.; Lim, C. Y.; Kroll, J. H.; Pierce, J. R.; Jathar, S. H., Oxygenated Aromatic Compounds are Important Precursors of Secondary Organic Aerosol in Biomass-Burning Emissions. *Environ. Sci. Technol.* **2020,** *54*, (14), 8568-8579.

20. Coggon, M. M.; Lim, C. Y.; Koss, A. R.; Sekimoto, K.; Yuan, B.; Gilman, J. B.; Hagan, D. H.; Selimovic, V.; Zarzana, K. J.; Brown, S. S.; Roberts, J. M.; Müller, M.; Yokelson, R.; Wisthaler, A.; Krechmer, J. E.; Jimenez, J. L.; Cappa, C.; Kroll, J. H.; de Gouw, J.; Warneke, C., OH chemistry of non-methane organic gases (NMOGs) emitted from laboratory and ambient biomass burning smoke: evaluating the influence of furans and oxygenated aromatics on ozone and secondary NMOG formation. *Atmos. Chem. Phys.* **2019,** *19*, (23), 14875-14899.

21. Jiang, J.; Carter, W. P. L.; Cocker, D. R.; Barsanti, K. C., Development and Evaluation of a Detailed Mechanism for Gas-Phase Atmospheric Reactions of Furans. *ACS Earth Space Chem.* **2020,** *4*, (8), 1254-1268.

22. Gómez Alvarez, E.; Borrás, E.; Viidanoja, J.; Hjorth, J., Unsaturated dicarbonyl products from the OH-initiated photo-oxidation of furan, 2-methylfuran and 3-methylfuran. *Atmos. Environ.* **2009,** *43*, (9), 1603-1612.

23. Joo, T.; Rivera-Rios, J. C.; Takeuchi, M.; Alvarado, M. J.; Ng, N. L., Secondary Organic Aerosol Formation from Reaction of 3-Methylfuran with Nitrate Radicals. *ACS Earth and Space*

Chem. **2019,** *3*, (6), 922-934.

24. Strollo, C. M.; Ziemann, P. J., Products and mechanism of secondary organic aerosol formation from the reaction of 3-methylfuran with OH radicals in the presence of NOx. *Atmos. Environ.* **2013,** *77*, 534-543.

25. Jiang, X.; Tsona, N. T.; Jia, L.; Liu, S.; Zhang, H.; Xu, Y.; Du, L., Secondary organic aerosol formation from photooxidation of furan: effects of NOx and humidity. *Atmos. Chem. Phys.* **2019,** *19*, (21), 13591-13609.

26. Cao, J., The Importance of Aerosols in the Earth System: Science and Engineering Perspectives. *Aerosol Sci. Eng.* **2017,** *1*, (1), 1-6.

27. Grace, D. N.; Sharp, J. R.; Holappa, R. E.; Lugos, E. N.; Sebold, M. B.; Griffith, D. R.; Hendrickson, H. P.; Galloway, M. M., Heterocyclic Product Formation in Aqueous Brown Carbon Systems. *ACS Earth Space Chem.* **2019,** *3*, (11), 2472-2481.

28. Jiang, H.; Frie, A. L.; Lavi, A.; Chen, J. Y.; Zhang, H.; Bahreini, R.; Lin, Y.-H., Brown Carbon Formation from Nighttime Chemistry of Unsaturated Heterocyclic Volatile Organic Compounds. *Environ. Sci. Technol. Lett.* **2019,** *6*, (3), 184-190.

29. Tsigaridis, K.; Kanakidou, M., Secondary organic aerosol importance in the future atmosphere. *Atmos. Environ.* **2007,** *41*, (22), 4682-4692.

30. Lambe, A. T.; Cappa, C. D.; Massoli, P.; Onasch, T. B.; Forestieri, S. D.; Martin, A. T.; Cummings, M. J.; Croasdale, D. R.; Brune, W. H.; Worsnop, D. R.; Davidovits, P., Relationship between Oxidation Level and Optical Properties of Secondary Organic Aerosol. *Environmental Science & Technology* **2013,** *47*, (12), 6349-6357.

31. Mayorga, R.; Chen, K.; Raeofy, N.; Woods, M.; Lum, M.; Zhao, Z.; Zhang, W.; Bahreini, R.; Lin, Y.-H.; Zhang, H., Chemical Structure Regulates the Formation of Secondary Organic Aerosol and Brown Carbon in Nitrate Radical Oxidation of Pyrroles and Methylpyrroles. *Environ. Sci. Technol.* **2022,** *56*, (12), 7761-7770.

32. Chen, K.; Raeofy, N.; Lum, M.; Mayorga, R.; Woods, M.; Bahreini, R.; Zhang, H.; Lin, Y.-H., Solvent effects on chemical composition and optical properties of extracted secondary brown carbon constituents. *Aerosol Sci. Tech.* **2022,** *56*, (10), 917-930.

33. Strand, T.; Larkin, N.; Rorig, M.; Krull, C.; Moore, M., PM2.5 measurements in wildfire smoke plumes from fire seasons 2005–2008 in the Northwestern United States. *J. Aerosol Sci.* **2011,** *42*, (3), 143-155.

34. Ding, Y.; Cruz, I.; Freedman, F.; Venkatram, A., Improving spatial resolution of PM2.5 measurements during wildfires. *Atmos. Pollut. Res.* **2021,** *12*, (5), 101047.

35. Decker, Z. C. J.; Zarzana, K. J.; Coggon, M.; Min, K.-E.; Pollack, I.; Ryerson, T. B.; Peischl, J.; Edwards, P.; Dubé, W. P.; Markovic, M. Z.; Roberts, J. M.; Veres, P. R.; Graus, M.; Warneke, C.; de Gouw, J.; Hatch, L. E.; Barsanti, K. C.; Brown, S. S., Nighttime Chemical Transformation in Biomass Burning Plumes: A Box Model Analysis Initialized with Aircraft Observations. *Environ. Sci. Technol.* **2019,** *53*, (5), 2529-2538.

36. Ziemann, P. J.; Atkinson, R., Kinetics, products, and mechanisms of secondary organic aerosol formation. *Chem. Soc. Rev.* **2012,** *41*, (19), 6582-6605.

37. Bahreini, R.; Keywood, M. D.; Ng, N. L.; Varutbangkul, V.; Gao, S.; Flagan, R. C.; Seinfeld, J. H.; Worsnop, D. R.; Jimenez, J. L., Measurements of Secondary Organic Aerosol from Oxidation of Cycloalkenes, Terpenes, and m-Xylene Using an Aerodyne Aerosol Mass Spectrometer. *Environ. Sci. Technol.* **2005,** *39*, (15), 5674-5688.

38. Lopez-Hilfiker, F. D.; Mohr, C.; Ehn, M.; Rubach, F.; Kleist, E.; Wildt, J.; Mentel, T. F.; Lutz, A.; Hallquist, M.; Worsnop, D.; Thornton, J. A., A novel method for online analysis of gas

and particle composition: description and evaluation of a Filter Inlet for Gases and AEROsols (FIGAERO). *Atmos. Meas. Tech.* **2014,** *7*, (4), 983-1001.

39. Zhang, X.; Zhang, H.; Xu, W.; Wu, X.; Tyndall, G. S.; Orlando, J. J.; Jayne, J. T.; Worsnop, D. R.; Canagaratna, M. R., Molecular characterization of alkyl nitrates in atmospheric aerosols by ion mobility mass spectrometry. *Atmos. Meas. Tech.* **2019,** *12*, (10), 5535-5545.

40. Zhao, Z.; Yang, X.; Lee, J.; Tolentino, R.; Mayorga, R.; Zhang, W.; Zhang, H., Diverse Reactions in Highly Functionalized Organic Aerosols during Thermal Desorption. *ACS Earth Space Chem.* **2020,** *4*, (2), 283-296.

41. Mayorga, R. J.; Zhao, Z.; Zhang, H., Formation of secondary organic aerosol from nitrate radical oxidation of phenolic VOCs: Implications for nitration mechanisms and brown carbon formation. *Atmos. Environ.* **2021,** *244*, 117910.

42. Dingle, J. H.; Zimmerman, S.; Frie, A. L.; Min, J.; Jung, H.; Bahreini, R., Complex refractive index, single scattering albedo, and mass absorption coefficient of secondary organic aerosols generated from oxidation of biogenic and anthropogenic precursors. *Aerosol Sci. Tech.* **2019,** *53*, (4), 449-463.

43. Frisch, M. J.; Trucks, G. W.; Schlegel, H. B.; Scuseria, G. E.; Robb, M. A.; Cheeseman, J. R.; Scalmani, G.; Barone, V.; Petersson, G. A.; Nakatsuji, H.; Li, X.; Caricato, M.; Marenich, A. V.; Bloino, J.; Janesko, B. G.; Gomperts, R.; Mennucci, B.; Hratchian, H. P.; Ortiz, J. V.; Izmaylov, A. F.; Sonnenberg, J. L.; Williams; Ding, F.; Lipparini, F.; Egidi, F.; Goings, J.; Peng, B.; Petrone, A.; Henderson, T.; Ranasinghe, D.; Zakrzewski, V. G.; Gao, J.; Rega, N.; Zheng, G.; Liang, W.; Hada, M.; Ehara, M.; Toyota, K.; Fukuda, R.; Hasegawa, J.; Ishida, M.; Nakajima, T.; Honda, Y.; Kitao, O.; Nakai, H.; Vreven, T.; Throssell, K.; Montgomery Jr., J. A.; Peralta, J. E.; Ogliaro, F.; Bearpark, M. J.; Heyd, J. J.; Brothers, E. N.; Kudin, K. N.; Staroverov, V. N.; Keith, T. A.; Kobayashi, R.; Normand, J.; Raghavachari, K.; Rendell, A. P.; Burant, J. C.; Iyengar, S. S.; Tomasi, J.; Cossi, M.; Millam, J. M.; Klene, M.; Adamo, C.; Cammi, R.; Ochterski, J. W.; Martin, R. L.; Morokuma, K.; Farkas, O.; Foresman, J. B.; Fox, D. J. *Gaussian 16 Rev. C.01*, Wallingford, CT, 2016.

44. Becke, A. D., Density-functional exchange-energy approximation with correct asymptotic behavior. *Physical Review A* **1988,** *38*, (6), 3098-3100.

45. Stephens, P. J.; Devlin, F. J.; Chabalowski, C. F.; Frisch, M. J., Ab Initio Calculation of Vibrational Absorption and Circular Dichroism Spectra Using Density Functional Force Fields. *The Journal of Physical Chemistry* **1994,** *98*, (45), 11623-11627.

46. Ditchfield, R.; Hehre, W. J.; Pople, J. A., Self‐Consistent Molecular‐Orbital Methods. IX. An Extended Gaussian‐Type Basis for Molecular‐Orbital Studies of Organic Molecules. *J. Chem. Phys.* **1971,** *54*, (2), 724-728.

47. Jacquemin, D.; Perpète, E. A.; Scuseria, G. E.; Ciofini, I.; Adamo, C., TD-DFT Performance for the Visible Absorption Spectra of Organic Dyes: Conventional versus Long-Range Hybrids. *J. Chem. Theory Comput.* **2008,** *4*, (1), 123-135.

48. Chen, J. Y.; Rodriguez, E.; Jiang, H.; Chen, K.; Frie, A.; Zhang, H.; Bahreini, R.; Lin, Y.-H., Time-Dependent Density Functional Theory Investigation of the UV–Vis Spectra of Organonitrogen Chromophores in Brown Carbon. *ACS Earth Space Chem.* **2020**.

49. Mennucci, B.; Cammi, R.; Tomasi, J., Excited states and solvatochromic shifts within a nonequilibrium solvation approach: A new formulation of the integral equation formalism method at the self-consistent field, configuration interaction, and multiconfiguration self-consistent field level. *J. Chem. Phys.* **1998,** *109*, (7), 2798-2807.

50. Singh, H. B.; Anderson, B. E.; Brune, W. H.; Cai, C.; Cohen, R. C.; Crawford, J. H.;

Cubison, M. J.; Czech, E. P.; Emmons, L.; Fuelberg, H. E.; Huey, G.; Jacob, D. J.; Jimenez, J. L.; Kaduwela, A.; Kondo, Y.; Mao, J.; Olson, J. R.; Sachse, G. W.; Vay, S. A.; Weinheimer, A.; Wennberg, P. O.; Wisthaler, A., Pollution influences on atmospheric composition and chemistry at high northern latitudes: Boreal and California forest fire emissions. *Atmos. Environ.* **2010,** *44*, (36), 4553-4564.

51. Decker, Z. C. J.; Robinson, M. A.; Barsanti, K. C.; Bourgeois, I.; Coggon, M. M.; DiGangi, J. P.; Diskin, G. S.; Flocke, F. M.; Franchin, A.; Fredrickson, C. D.; Gkatzelis, G. I.; Hall, S. R.; Halliday, H.; Holmes, C. D.; Huey, L. G.; Lee, Y. R.; Lindaas, J.; Middlebrook, A. M.; Montzka, D. D.; Moore, R.; Neuman, J. A.; Nowak, J. B.; Palm, B. B.; Peischl, J.; Piel, F.; Rickly, P. S.; Rollins, A. W.; Ryerson, T. B.; Schwantes, R. H.; Sekimoto, K.; Thornhill, L.; Thornton, J. A.; Tyndall, G. S.; Ullmann, K.; Van Rooy, P.; Veres, P. R.; Warneke, C.; Washenfelder, R. A.; Weinheimer, A. J.; Wiggins, E.; Winstead, E.; Wisthaler, A.; Womack, C.; Brown, S. S., Nighttime and daytime dark oxidation chemistry in wildfire plumes: an observation and model analysis of FIREX-AQ aircraft data. *Atmos. Chem. Phys.* **2021,** *21*, (21), 16293-16317.

52. Atkinson, R.; Aschmann, S. M.; Carter, W. P. L., Kinetics of the reactions of O3 and OH radicals with furan and thiophene at 298 ± 2 K. *Int. J. Chem. Kinet.* **1983,** *15*, (1), 51-61.

53. Atkinson, R.; Aschmann, S. M.; Winer, A. M.; Carter, W. P. L., Rate constants for the gas-phase reactions of nitrate radicals with furan, thiophene, and pyrrole at 295 .+-. 1 K and atmospheric pressure. *Environ. Sci. Technol.* **1985,** *19*, (1), 87-90.

54. Newland, M. J.; Ren, Y.; McGillen, M. R.; Michelat, L.; Daële, V.; Mellouki, A., NO3 chemistry of wildfire emissions: a kinetic study of the gas-phase reactions of furans with the NO3 radical. *Atmos. Chem. Phys.* **2022,** *22*, (3), 1761-1772.

55. Draper, D. C.; Farmer, D. K.; Desyaterik, Y.; Fry, J. L., A qualitative comparison of secondary organic aerosol yields and composition from ozonolysis of monoterpenes at varying concentrations of NO2. *Atmos. Chem. Phys.* **2015,** *15*, (21), 12267-12281.

56. Berndt, T.; Böge, O.; Rolle, W., Products of the Gas-Phase Reactions of NO3 Radicals with Furan and Tetramethylfuran. *Environ. Sci. Technol.* **1997,** *31*, (4), 1157-1162.

57. Zhang, W.; Wang, T.; Du, B.; Mu, L.; Feng, C., Mechanism for the gas-phase reaction between NO3 and furan: A theoretical study. *Chem. Phys. Lett.* **2008,** *455*, (4), 164-168.

58. Farmer, D. K.; Matsunaga, A.; Docherty, K. S.; Surratt, J. D.; Seinfeld, J. H.; Ziemann, P. J.; Jimenez, J. L., Response of an aerosol mass spectrometer to organonitrates and organosulfates and implications for atmospheric chemistry. *PNAS* **2010,** *107*, (15), 6670.

59. Day, D. A.; Campuzano-Jost, P.; Nault, B. A.; Palm, B. B.; Hu, W.; Guo, H.; Wooldridge, P. J.; Cohen, R. C.; Docherty, K. S.; Huffman, J. A.; de Sá, S. S.; Martin, S. T.; Jimenez, J. L., A systematic re-evaluation of methods for quantification of bulk particle-phase organic nitrates using real-time aerosol mass spectrometry. *Atmos. Meas. Tech.* **2022,** *15*, (2), 459-483.

60. Cao, G.; Yan, Y.; Zou, X.; Zhu, R.; Ouyang, F., Applications of Infrared Spectroscopy in Analysis of Organic Aerosols. *Spectr. Anal. Rev.* **2018,** *06*, 12-32.

61. Jang, M.; Czoschke Nadine, M.; Lee, S.; Kamens Richard, M., Heterogeneous Atmospheric Aerosol Production by Acid-Catalyzed Particle-Phase Reactions. *Science* **2002,** *298*, (5594), 814-817.

62. Leito, I.; Herodes, K.; Huopolainen, M.; Virro, K.; Künnapas, A.; Kruve, A.; Tanner, R., Towards the electrospray ionization mass spectrometry ionization efficiency scale of organic compounds. *Rapid Commun. Mass Spectrom.* **2008,** *22*, (3), 379-384.

63. Oss, M.; Kruve, A.; Herodes, K.; Leito, I., Electrospray Ionization Efficiency Scale of Organic Compounds. *Anal. Chem.* **2010,** *82*, (7), 2865-2872.

64. Kodros, J. K.; Papanastasiou, D. K.; Paglione, M.; Masiol, M.; Squizzato, S.; Florou, K.; Skyllakou, K.; Kaltsonoudis, C.; Nenes, A.; Pandis, S. N., Rapid dark aging of biomass burning as an overlooked source of oxidized organic aerosol. *PNAS* **2020,** *117*, (52), 33028.
65. Tsigaridis, K.; Kanakidou, M., The Present and Future of Secondary Organic Aerosol Direct Forcing on Climate. *Curr. Clim. Change Rep.* **2018,** *4*, (2), 84-98.
66. Akagi, S. K.; Craven, J. S.; Taylor, J. W.; McMeeking, G. R.; Yokelson, R. J.; Burling, I. R.; Urbanski, S. P.; Wold, C. E.; Seinfeld, J. H.; Coe, H.; Alvarado, M. J.; Weise, D. R., Evolution of trace gases and particles emitted by a chaparral fire in California. *Atmos. Chem. Phys.* **2012,** *12*, (3), 1397-1421.
67. Westerling, A. L.; Gershunov, A.; Brown, T. J.; Cayan, D. R.; Dettinger, M. D., Climate and Wildfire in the Western United States. *Bull. Amer. Meteor. Soc.* **2003,** *84*, (5), 595-604.
68. Holden Zachary, A.; Swanson, A.; Luce Charles, H.; Jolly, W. M.; Maneta, M.; Oyler Jared, W.; Warren Dyer, A.; Parsons, R.; Affleck, D., Decreasing fire season precipitation increased recent western US forest wildfire activity. *PNAS* **2018,** *115*, (36), E8349-E8357.
69. Jiang, Y.; Zhou, L.; Raghavendra, A., Observed changes in fire patterns and possible drivers over Central Africa. *Environ. Res. Lett.* **2020,** *15*, (9), 0940b8.
70. Ramo, R.; Roteta, E.; Bistinas, I.; van Wees, D.; Bastarrika, A.; Chuvieco, E.; van der Werf Guido, R., African burned area and fire carbon emissions are strongly impacted by small fires undetected by coarse resolution satellite data. *PNAS* **2021,** *118*, (9), e2011160118.
71. Zhang, Y.; Forrister, H.; Liu, J.; Dibb, J.; Anderson, B.; Schwarz, J. P.; Perring, A. E.; Jimenez, J. L.; Campuzano-Jost, P.; Wang, Y.; Nenes, A.; Weber, R. J., Top-of-atmosphere radiative forcing affected by brown carbon in the upper troposphere. *Nat. Geosci.* **2017,** *10*, (7), 486-489.
72. Lang, T.; Buehler, S. A.; Burgdorf, M.; Hans, I.; John, V. O., A new climate data record of upper-tropospheric humidity from microwave observations. *Sci. Data* **2020,** *7*, (1), 218.
73. Yan, C.; Zheng, M.; Desyaterik, Y.; Sullivan, A. P.; Wu, Y.; Collett Jr, J. L., Molecular Characterization of Water-Soluble Brown Carbon Chromophores in Beijing, China. *J. Geophys. Res. Atmos.* **2020,** *125*, (15), e2019JD032018.
74. Li, X.; Hu, M.; Wang, Y.; Xu, N.; Fan, H.; Zong, T.; Wu, Z.; Guo, S.; Zhu, W.; Chen, S.; Dong, H.; Zeng, L.; Yu, X.; Tang, X., Links between the optical properties and chemical compositions of brown carbon chromophores in different environments: Contributions and formation of functionalized aromatic compounds. *Sci. Total Environ.* **2021,** *786*, 147418.
75. Sun, Y.; Tang, J.; Mo, Y.; Geng, X.; Zhong, G.; Yi, X.; Yan, C.; Li, J.; Zhang, G., Polycyclic Aromatic Carbon: A Key Fraction Determining the Light Absorption Properties of Methanol-Soluble Brown Carbon of Open Biomass Burning Aerosols. *Environ. Sci. Technol.* **2021,** *55*, (23), 15724-15733.
76. Schauer, J. J.; Fraser, M. P.; Cass, G. R.; Simoneit, B. R. T., Source Reconciliation of Atmospheric Gas-Phase and Particle-Phase Pollutants during a Severe Photochemical Smog Episode. *Environ. Sci. Technol.* **2002,** *36*, (17), 3806-3814.
77. Zheng, M.; Cass, G. R.; Schauer, J. J.; Edgerton, E. S., Source Apportionment of PM2.5 in the Southeastern United States Using Solvent-Extractable Organic Compounds as Tracers. *Environ. Sci. Technol.* **2002,** *36*, (11), 2361-2371.
78. Fine, P. M.; Chakrabarti, B.; Krudysz, M.; Schauer, J. J.; Sioutas, C., Diurnal Variations of Individual Organic Compound Constituents of Ultrafine and Accumulation Mode Particulate Matter in the Los Angeles Basin. *Environ. Sci. Technol.* **2004,** *38*, (5), 1296-1304.
79. Ikemori, F.; Nakayama, T.; Hasegawa, H., Characterization and possible sources of nitrated mono- and di-aromatic hydrocarbons containing hydroxyl and/or carboxyl functional groups in

ambient particles in Nagoya, Japan. *Atmos. Environ.* **2019,** *211*, 91-102.